Shock Waves (2009) 19:521–530
DOI 10.1007/s00193-009-0234-6

ORIGINAL ARTICLE

Separation control by vortex generator devices in a transonic channel flow

Reynald Bur · Didier Coponet · Yves Carpels

Received: 4 February 2009 / Revised: 10 July 2009 / Accepted: 1 October 2009 / Published online: 23 October 2009

Abstract An experimental study was conducted in a transonic channel to control by mechanical vortex generator devices the strong interaction between a shock wave and a separated turbulent boundary layer. Control devices—co-rotating and counter-rotating vane-type vortex generators—were implemented upstream of the shock foot region and tested both on a steady shock wave and on a forced shock oscillation configurations. The spanwise spacing of vortex generator devices along the channel appeared to be an important parameter to control the flow separation region. When the distance between each device is decreased, the vortices merging is more efficient to reduce the separation. Their placement upstream of the shock wave is determinant to ensure that vortices have mixed momentum all spanwise long before they reach the separation line, so as to avoid separation cells. Then, vortex generators slightly reduced the amplitude of the forced shock wave oscillation by delaying the upstream displacement of the leading shock.

Keywords Transonic flow · Shock wave · Boundary layer · Separated flow · Vortex generator

PACS 47.27.nd · 47.40.Nm · 47.32.Ff · 47.85.L−

1 Introduction

Both external and internal flows are often the subject of shock waves, which interact strongly with turbulent boundary layers. The result is frequently the formation of separation with always negative consequences: drag penalty, fall of efficiency and high amplitude fluctuations related to the development of large turbulent structures in the separated zones of the flow. This leads to decrease the performance of a supercritical wing aircraft and to limit the efficiency of supersonic aircraft or missile propulsion systems.

Thus, mechanical vortex generator devices (VGs) allowing momentum transfer have been successfully used for a long time to delay flow separation [1]. They introduced vorticity of an appropriate sign and direction and increased the mixing between the upper and lower layers of the turbulent boundary layer. Recent reviews [2–4] on flow control technology associated with their range of applicability have given a list of vortex generator devices tested to control the boundary layer separation. They may take the form of vanes or obstacles, air jets or mass-less jets. Nevertheless, control of shock-induced separation by such vortex generator devices is not widely discussed in the literature. McCormick's experiments [5] revealed that sub boundary layer doublet VGs (its height h is equal to 0.36 the incoming boundary layer thickness δ) significantly suppress the shock-induced separation bubble and improve the boundary layer properties downstream of the shock. However, he noticed a wave drag penalty due to the modification of the shock pattern from a λ-foot shock system to a quasi-normal shock wave. Ashill et al. [6] reported tests on a transonic airfoil equipped with several VGs devices. The sub counter-rotating vane-type VGs (h at the scale of the boundary layer displacement thickness δ^*) produced a 20% increase of the maximum lift when their location towards the shock position is well chosen; i.e., $70\,h$ upstream of the shock. The choice of the distance between the VGs and the interaction region to efficiently control the shock-induced separation is well evidenced by Babinsky et al. [7]. It was observed that the most

Communicated by J.-P. Dussauge.

R. Bur (✉) · D. Coponet · Y. Carpels
Fundamental and Experimental Aerodynamics Department,
ONERA, 92190 Meudon, France
e-mail: Reynald.Bur@onera.fr

efficient location of micro counter-rotating vane-type VGs (around 20% of the incoming boundary layer thickness δ) depends on the nominal (diffuser entry) Mach number. When the Mach number is increased, a downstream placement of the VGs closer to the separation onset was found to be more beneficial.

The purpose of the present experimental study is to control by mechanical (passive) vortex generator devices the strong interaction between a shock wave and a separated turbulent boundary layer in a transonic channel. Control devices—co-rotating and counter-rotating vane-type VGs—are implemented upstream of the shock foot region and are tested both on a steady shock wave and on a forced shock oscillation configurations.

2 Experimental conditions and means of investigation

2.1 Wind tunnel and flow conditions

Experiments were performed in the S8Ch wind tunnel of the ONERA Meudon Center. This facility is a continuous wind tunnel supplied with desiccated atmospheric air. The transonic channel is 100 mm high and has a span of 120 mm at the entrance of the test section (see Fig. 1). The test set-up consists of a rectilinear upper wall and a lower wall equipped with a contour profile (bump). The shape of the bump has been specially designed to induce a strong interaction between the boundary layer and the shock when it takes place at the level of the rear part of the bump, the nominal Mach number being equal to 1.45. Such an interaction induced an extended separated zone.

The stagnation conditions were near ambient pressure and temperature: $p_{st} = 0.96 \times 10^5 \pm 300$ Pa and $T_{st} = 300 \pm 10$ K. Probing using a two-component laser Doppler velocimetry (LDV) system has been performed in the front part of the bump, where the flow is still subsonic, in order to give inlet flow conditions for computations [8]. At the station $X = 135$ mm (see Fig. 4 for the definition of the co-ordinate system), the boundary layer on the bump is fully turbulent with the following characteristics: physical thickness $\delta = 4$ mm, displacement thickness $\delta^* = 0.46$ mm, momentum thickness $\theta = 0.25$ mm, and incompressible shape parameter $H_i = 1.6$. The associated unit Reynolds number is around $14 \times 10^6\,\mathrm{m}^{-1}$, which leads to a value of $Re_\theta = 3500$ for the incoming flow. Moreover, previous experiments on the same configuration have allowed to determine the boundary layer properties at the beginning of the rear part of the bump, upstream of the interaction region [9]. These properties are very similar to those obtained in the converging part of the channel, the pressure gradients being weak in the bump crest region (sonic flow condition).

Fig. 1 Photograph of the test set-up in the S8Ch wind tunnel

Nearly sinusoidal pressure perturbations were introduced at the downstream end of the channel by periodic variation of the second throat section thanks to a rotating elliptical shaft located near this throat, in the middle of the channel [10]. This device caused forced shock-wave oscillations at a known adjustable frequency. In these experiments, the shock oscillation frequency is equal to 30 Hz, which produces a shock oscillation amplitude of around 30 mm. Similar experimental studies on shock response to downstream perturbations were performed by Sajben et al. [11,12] and Ott et al. [13].

2.2 Vortex generator devices

The mechanical vane-type vortex generators were triangular elements whose angular position is fixed at 18° with regard to the main flow direction. It is consistent with the results of Pauley et al. [14] who observed a linear increase of the vortices strength up to an angle of 18°. Several parameters have been tested both for co-rotating VGs and counter-rotating VGs (see Fig. 2). An important parameter to take into account in the study is the VGs height h, as referred to in previous studies [3,4,15]. Then, conventional VGs (with $h/\delta = 1$, noted CoC and C) have been compared to sub-VGs (with $h/\delta = 0.5$, noted CoS and S). Concerning the counter-rotating VGs, the effect of spacing between each couple of VGs have been tested ($\lambda/h = 10$ and 5, respectively, for the devices C1, S1 and C2, S2).

Moreover, the number of VGs has been adapted for each configuration in order to cover the entire span of the test set-up. The VGs devices are located along a line situated at 10 mm downstream of the bump crest. This position has been selected thanks to 3D numerical simulations carried out to optimize the efficiency of VGs to delay the separation [16]. It corresponds to a distance upstream of the shock foot equal to 32δ for the sub-VGs (16δ for the conventional VGs), which is in the range of values found in the literature [3–7]. Finally,

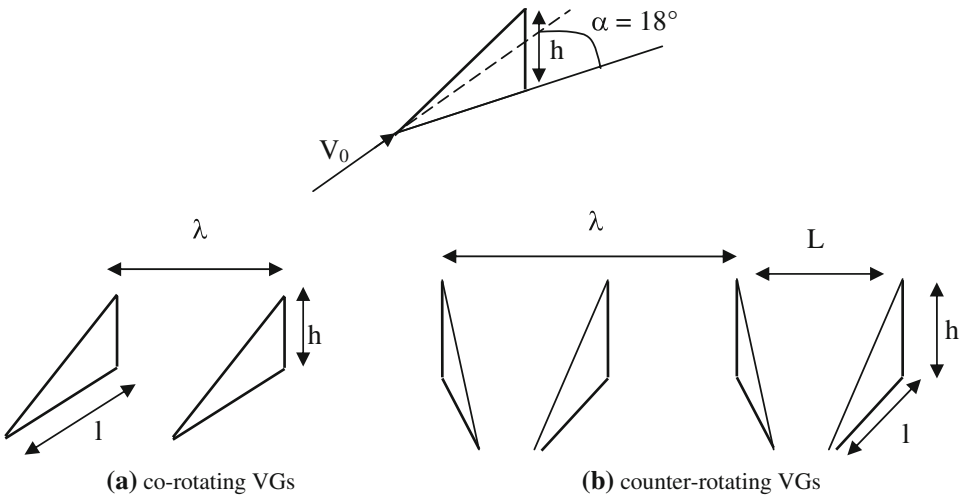

Fig. 2 Definition of the vane-type vortex generators

(a) co-rotating VGs **(b)** counter-rotating VGs

Table 1 Geometrical parameters of the vane-type vortex generators

	Co-rotating VGs		Counter-rotating VGs			
	CoC1	CoS1	C1	C2	S1	S2
h/δ	1	0.5	1	1	0.5	0.5
l/h	2.5	2.5	2.5	1.25	2.5	1.25
L/h	–	–	3	1.5	3	1.5
λ/h	6	6	10	5	10	5
Number	5	9	3	5	5	11

six configurations of vane-type vortex generators were under study in these experiments (see Table 1; Fig. 3).

One notices that the efficiency of these VGs devices to control the shock-induced separation should be compared to passive and active bleed devices tested in a previous study. This device consisted of a cavity covered by a perforated plate placed in the interaction region. Passive control is defined by a natural flow recirculation through the cavity and active control means flow suction through the perforated plate [10].

2.3 Flow visualizations

A schlieren apparatus was used to visualize the flow field and control the shock wave positions in the test section. It used a conventional z-type mirror system with a horizontal knife edge. The recording device is a high-speed camera Phantom V7.0 coupled with HBO light. The high-speed camera characteristics are a resolution of 800 × 400 pixels and an acquisition speed of 4,000 frames per second.

Laser sheet visualizations and oil flow visualizations—by means of coloured viscous coat—were performed to allow tracking of the trajectories of the small-scale streamwise vortices emanating from the VG devices and their interaction with the boundary layer and the shock wave. For the laser sheet visualizations, the set-up used is a Millenia Spectra Physics diode pump laser, with a 5-W light power. The wave length of the light is $\lambda = 532 \times 10^{-3}$ µm, which corresponds to the green colour. The flow was seeded by synthetic smoke (Pro-Smoke Super Fluid containing polyglycols) emanating from the settling chamber of the wind tunnel. Concerning oil flow visualizations, viscous coat is applied before each test along the span of the test section just upstream of the VG devices.

2.4 Pressure taps and sensors

The lower wall of the test set-up was equipped with 39 continuous pressure taps located on a line at 10 mm from the median plane and six unsteady pressure sensors (named P and G) located on the median plane, primarily in the interaction region. Figure 4 shows their distributions along the lower wall of the channel.

The continuous pressure taps have a diameter of 0.4 mm and are connected to Statham^{TM} transducers via rubber tubes. The unsteady pressure transducers are absolute or differential 15psi Kulite^{TM} XCS093 sensors with a diameter of 0.8 mm. Pressure measurement uncertainties are ±800 Pa for the Statham^{TM} transducers and ±105 Pa for the Kulite^{TM} sensors, respectively.

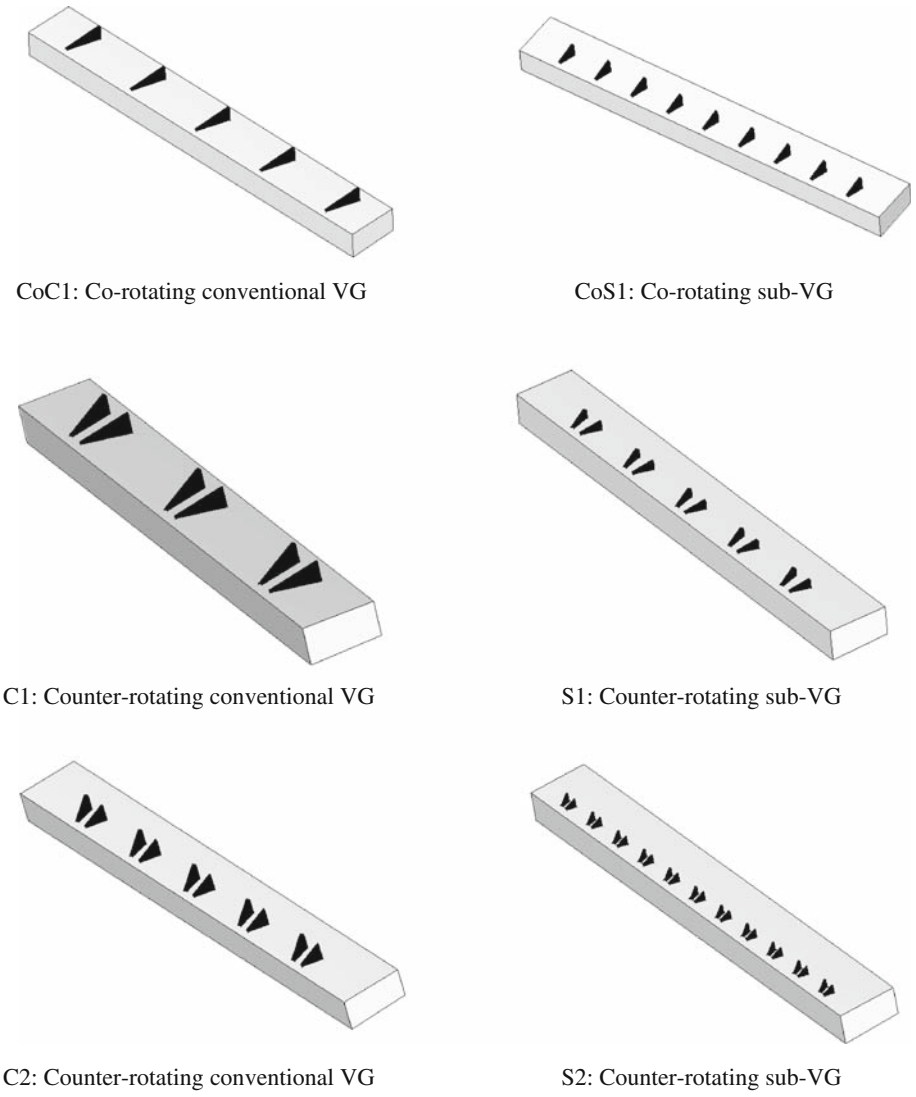

Fig. 3 Configurations of the vane-type vortex generators under study

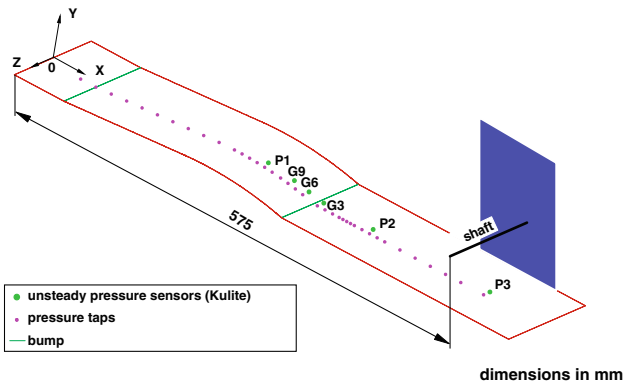

Fig. 4 Sketch of the pressure taps and Kulite sensors positions along the lower wall of the channel

The origin of the co-ordinate system is at the beginning of the lower wall (see Fig. 4). The X-axis is along the lower wall in the streamwise direction, Y is normal to the lower wall and the bump chord and Z is along the spanwise direction ($Z = 0$ in the median plane). The origin of the bump is at $X = 65$ mm. Its length is 286.4 mm and its crest 12 mm. The VG devices are located at $X = 261.4$ mm, 10 mm downstream of the bump crest.

3 Results for the steady shock wave configuration

3.1 Schlieren visualizations

Figure 5 compares the schlieren visualizations between the reference case without control and the control case with counter-rotating VG-C2. In the reference case (see Fig. 5a), the interaction region is characterized by a large λ-shock structure in the core flow. The oblique leading shock, downstream of which the Mach number is still supersonic, and the trailing shock meet at the triple point from which starts the

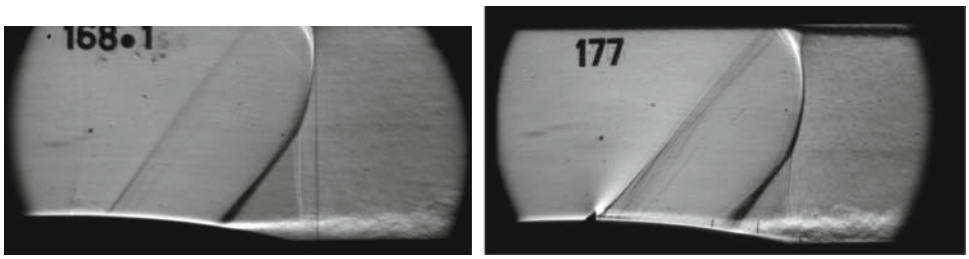

(a) reference case **(b)** VG-C2

Fig. 5 Schlieren visualizations for steady shock wave configuration without control **(a)** and with VG-C2 device **(b)**

single strong shock. The boundary layer is destabilized with massive separation and large vortex structures are developed in the shear stress layer. The wave visible upstream of the interaction region is created by the junction between the bump and the insert manufactured for the clean case, like those of Fig. 3 without VGs. However, the intensity of this wave is very weak and does not generate perturbation in the interaction region [8]. For the control case (see Fig. 5b), the size of the λ-shock structure is reduced compared to the reference case, the position of the triple point being lower in the channel. The trails of the vortices generated by the VGs are observed near the curved wall. The extension of the separation region is reduced under the effects of VGs and the shear layer is growing. The presence of VGs generates expansion waves followed by moderate compression waves in the channel flowfield.

3.2 Wall pressure distributions

The lower wall pressure distributions are plotted in Fig. 6 for the reference case without control and the six VG devices. The reference case distribution reveals the existence of a large separation region corresponding to a quasi-plateau pressure level after the intense recompression of the flow. According to previous experiments with LDV measurements [8,10], the separation point is located near $X = 328$ mm and the reattachment point around $X = 390$ mm. When control by VGs is applied, the plateau pressure seems to disappear and the efficiency of VGs to delay the separation region increases when the spacing between VGs is decreasing (S2 compared to S1, C2 to C1). Then, the VG-S2 device (11 pairs of counter-rotating sub-vortex generators) seems to suppress the separation in the near-median plane of the test section. For this configuration with a large number of VGs in the spanwise direction, previous numerical simulations have indicated that the pairs of vortices emanating from each VG do not merge in the boundary layer upstream of the interaction region [16].

The flow perturbations—expansion and compression waves observed on schlieren visualization (see Fig. 5b)—generated by the VGs have a slight intensity and only have a local effect on the pressure distributions. In term of drag penalties, the way to reduce the effects of these perturbations

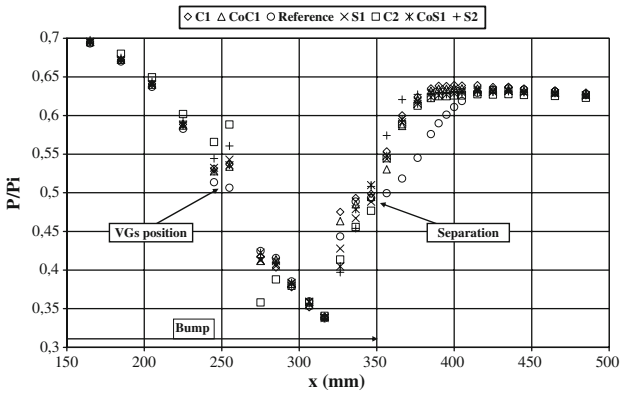

Fig. 6 Wall pressure distributions for steady shock wave configuration without control and with VG devices

is to impose the height of the VGs at a value less than the sonic line of the incoming boundary layer [5–7]. Probing of the boundary layer on the rear part of the bump, upstream of the interaction region, has allowed to determine sonic condition at $h^* = 0.5$ mm [9]. In these experiments, the height of the tested VG devices is always greater than the location of the sonic line; i.e., $h/h^* = 8$ and 4 for the conventional and sub-VGs, respectively.

3.3 Laser sheet visualizations

Figure 7 shows laser sheet visualizations for four spanwise planes located between the conventional counter-rotating VG-C2 device and the separation flow region. In the first plane located in the near-wake of the VG device (see Fig. 7a), one can observe the birth of pair of vortices emanating from the VGs, with a singular comma-shape due to the triangular surface of the VGs. In the plane located at 5δ downstream of VGs (see Fig. 7b), well-formed vortices are convected inside the boundary layer, as already observed in the schlieren picture of Fig. 5b. For the plane located at 15δ downstream of VGs, near the shock foot region (see Fig. 7c), the distance between two vortices (generated by a VG device) is growing compared to those of the previous planes. Considering the last plane located inside the separation region (see Fig. 7d), one notices a significant modification of the near-wall flow pattern. Due to the presence of shock waves, the size of the

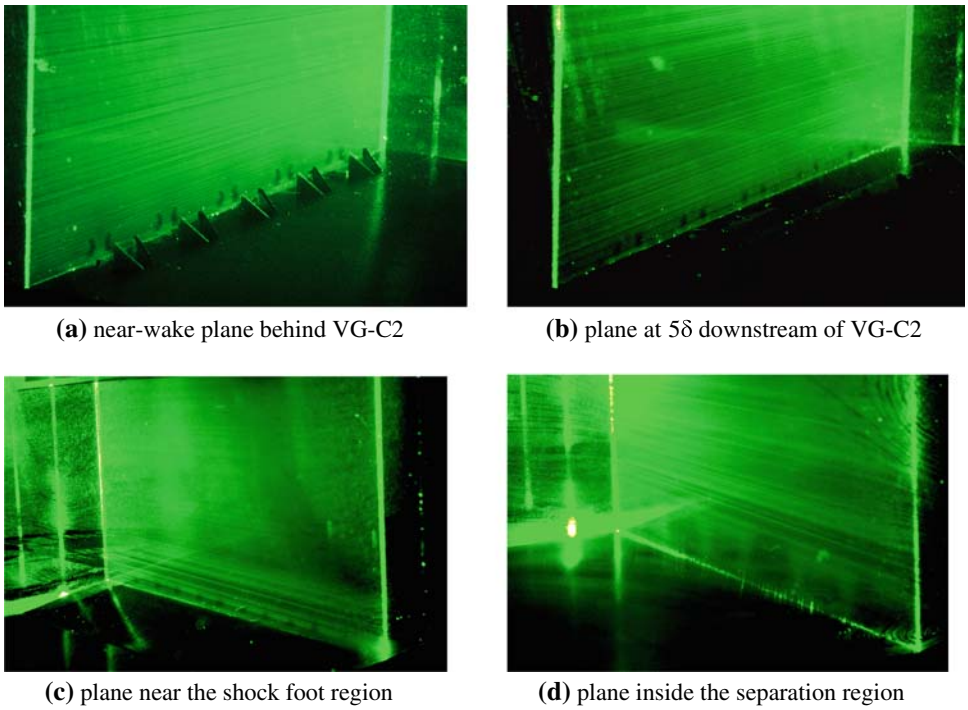

(a) near-wake plane behind VG-C2 **(b)** plane at 5δ downstream of VG-C2

(c) plane near the shock foot region **(d)** plane inside the separation region

Fig. 7 Laser sheet visualizations for steady shock wave configuration—spanwise planes located between the VG-C2 device and the separation region

vortices is increased; the vorticity rate is modified due to the reduction of the axial velocity after the crossing of vortices through the shock system. Their trajectories are slightly changed, but the distance between vortices is still increasing; then, a vortex emanating from a VG device is merging with a vortex issuing from the next VG to form a large vortex structure (see in the plane the black pockets without seeding particles). This mechanism allows to catch the flow from the upper layer of the boundary layer to the less energetic inner layer and, then, to strongly reduce the separation region of the flow.

3.4 Oil flow visualizations

Coloured oil flow visualizations have been performed for the steady shock wave configurations without control and with several VG devices. A comparison between the reference case (see Fig. 8a) and the control case with VG-C2 device (see Fig. 8b) allows to notice an important modification of the flow separation pattern: the separation line located in the rear part of the bump is replaced by a corrugated separated line due to the presence of intense vortices. The flow seems to be partially reattached under the action of VGs vortices. The merging of vortices created by two close VG devices to form large vortex structures is evidenced by their footprints on the lower wall. For the VG-C2 device, the four vortex footprints are corresponding to the four black pockets observed by laser sheet visualization (see Fig. 7d). The effect of VG height is discussed by a comparison between the conventional VG-C2 (see Fig. 8b) and the sub-VG-S1 (see Fig. 8c). The VG height seems to have a slight influence on the flow topology, especially on flow separation extension. One notes a significant interaction with corner flows, which are not controlled in this study. Then, a comparison between counter-rotating VG-S1 (see Fig. 8c) and co-rotating VG-CoS1 (see Fig. 8d) shows that a non symmetrical flow topology is obtained for the co-rotating VGs with smaller footprints of vortices at the wall. This co-rotating VGs configuration is more adapted to control a full 3-D flow, for instance, on a swept wing. The skin friction lines pattern near the leading edge of the wing leads to choose an averaged value for the VGs angular position regarding the upstream flow direction, which is easier to achieve with co-rotating VGs device [6,17].

4 Results for the forced shock oscillation configuration

4.1 Schlieren visualizations

Figure 9 shows the extreme positions of the shock wave in the channel for the shock oscillation frequency of 30 Hz, considering the reference case without control. The corresponding shock oscillation amplitude is equal to 30 mm. The shock positions in the channel are estimated in the core flow, at $Y = 75$ mm, where the shock wave is nearly normal. The interaction region is characterized by a large λ-shock structure in the core flow. The behaviour of the boundary layer is different between these two shock positions: in the upstream position, the boundary layer is separated with important vortex structures in the shear layer; in the down-

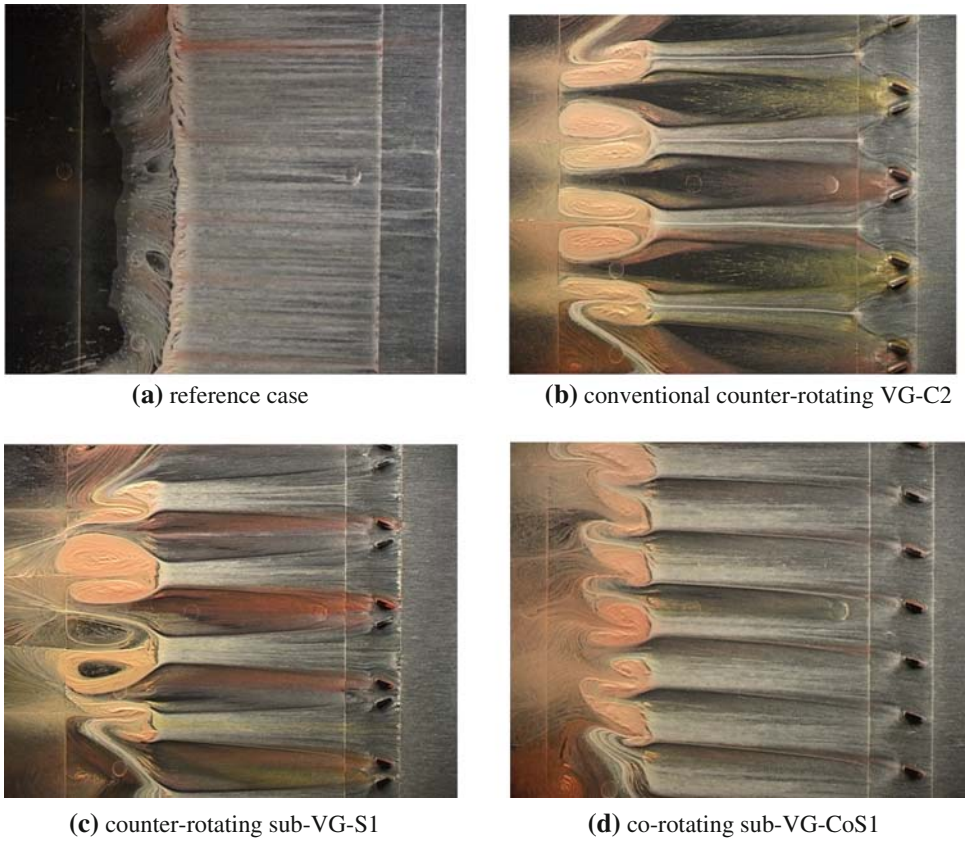

(a) reference case **(b)** conventional counter-rotating VG-C2

(c) counter-rotating sub-VG-S1 **(d)** co-rotating sub-VG-CoS1

Fig. 8 Oil flow visualizations for steady shock wave configuration without control and with several VG devices (direction of the flow is *right-to-left*)

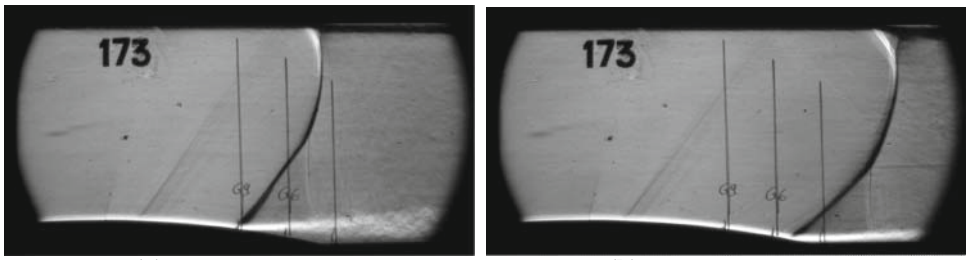

(a) upstream position **(b)** downstream position

Fig. 9 Schlieren visualizations for 30 Hz-forced shock oscillation configuration—reference case without control

stream position, the boundary layer is attached. More in-depth analysis of the flowfield was obtained in a previous study by LDV probing with phase-averaged technique using time information given by a marker placed on the rotating shaft [8,10].

4.2 Unsteady pressure measurements

Figure 10 shows the longitudinal evolution of the pressure fluctuations spectra obtained from signals measured by sensors located in the test section median plane, at the 30 Hz shock oscillation, for the reference case without control. These spectra are represented in sound pressure level (SPL) expressed in dB, by

$$\mathrm{SPL(dB)} = 20 \times \log_{10}\left(\frac{\sqrt{S_{p'p'}}}{p_{\mathrm{ref}}}\right)$$

where $S_{p'p'}$ is the spectrum modulus, in Pa^2, and p_{ref} is equal to 2×10^{-5} Pa. The sample frequency is 6,000 Hz for each sensor; the spectrum average is obtained from 50 blocks and 8,192 samples.

The P1 sensor spectrum (at $X = 281.4$ mm) exhibits no particular frequencies because it is located in the supersonic zone of the flow and is not sensible to downstream perturbations. The G9 sensor (at $X = 316.4$ mm) gives a peak at the shock oscillation fundamental frequency $f = 30$ Hz, and some harmonics. These peaks have a weak intensity because

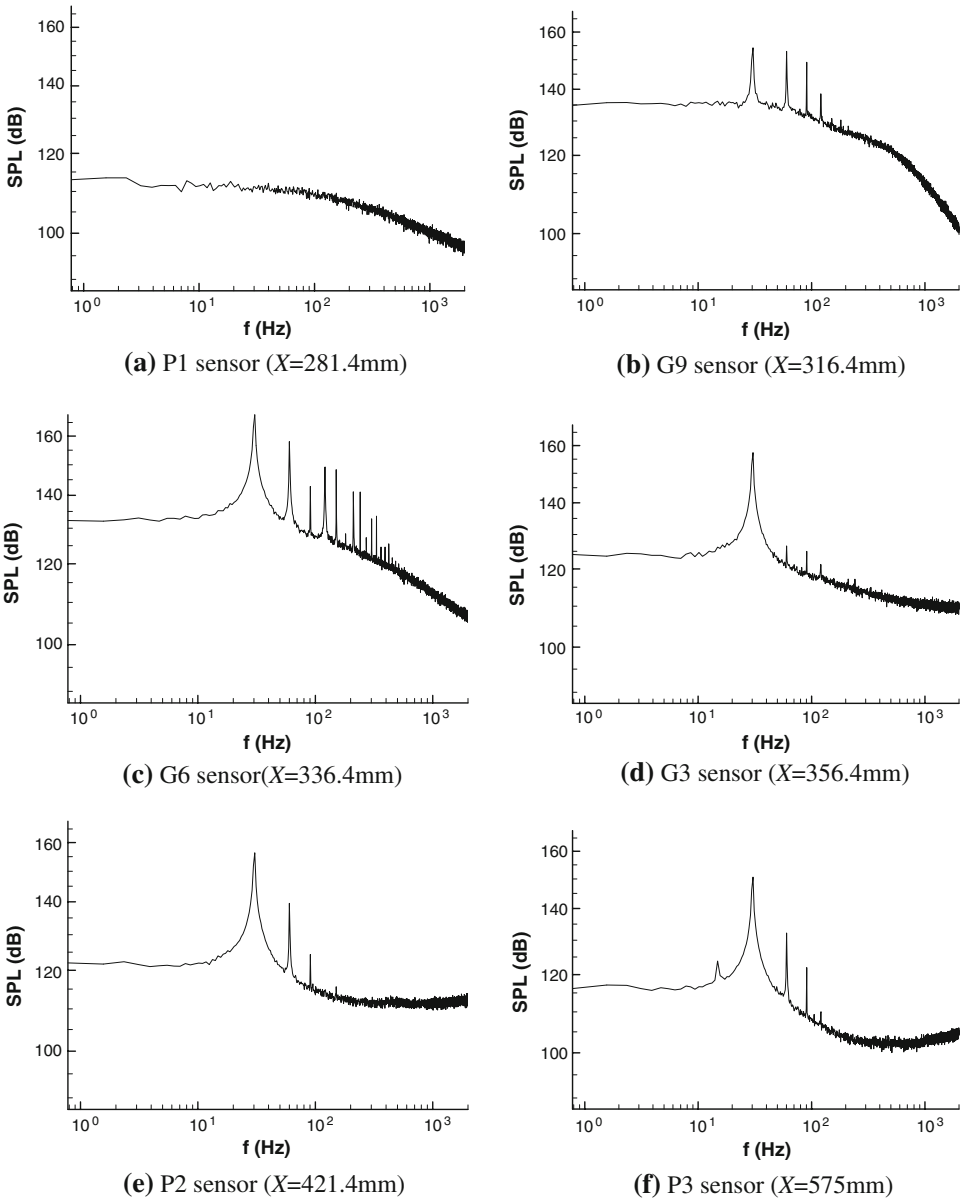

(a) P1 sensor (X=281.4mm) **(b)** G9 sensor (X=316.4mm)

(c) G6 sensor(X=336.4mm) **(d)** G3 sensor (X=356.4mm)

(e) P2 sensor (X=421.4mm) **(f)** P3 sensor (X=575mm)

Fig. 10 Longitudinal evolution of the pressure fluctuations spectra for 30 Hz-forced shock oscillation configuration—reference case without control

this sensor is in border of the shock wave oscillation. The G6 sensor (at $X = 336.4$ mm) has several harmonics and the fundamental peak very energetic (at $f = 30$ Hz). This sensor picks up very well the shock wave oscillation. The G3 sensor (at $X = 356.4$ mm, just downstream of the bump) gives the fundamental peak (at $f = 30$ Hz) and very weak harmonics. The fundamental peak is less energetic than that of the G6 sensor (158 dB instead of 168 dB). This can be explained by the location of the sensor. Indeed, according to the schlieren visualizations (see Fig. 9), this sensor is always located downstream of the leading shock, so all the harmonics have nearly disappeared. The P2 sensor (at $X = 421.4$ mm) and P3 sensor (at $X = 575$ mm, under the shaft) have almost the same spectrum. These two sensors, which are located in the subsonic zone, are mainly sensible to the downstream pressure perturbations.

Comparisons between the reference case and control cases with VG devices, for the 30 Hz forced shock oscillation configuration, are carried out on the evolution of the pressure fluctuations, respectively, for their RMS levels (see Fig. 11) and spectra (see Fig. 12, only for the three sensors located in the shock oscillation region and with the VG-C2 device). Concerning the G9 sensor, control by VGs allows to maintain the RMS pressure level at the level measured in the upstream supersonic region (P1 sensor), whereas this level is strongly increased without control. So, the extreme location of the leading shock of the λ-shock structure is moving in the downstream direction due to VGs effects, which leads to a

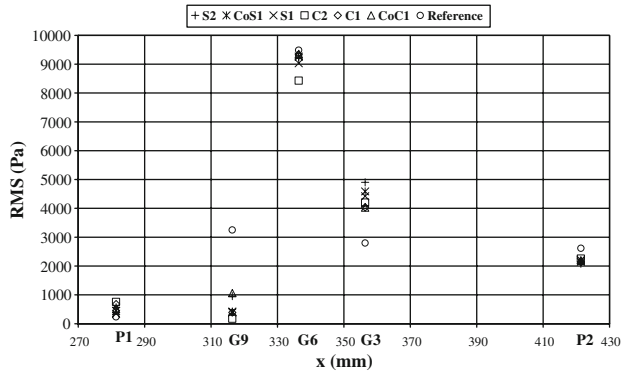

Fig. 11 RMS pressure levels for 30 Hz-forced shock oscillation configuration without control and with VG devices

reduction of the shock oscillation amplitude. The corresponding spectrum for the VG-C2 device (see Fig. 12a) has a lesser broadband level (−25 dB) compared to the reference case one, similar to that of the supersonic region (see Fig. 10a). The presence of weak peaks means that the upstream location of the leading shock is at the limit of the sensor location. Nevertheless, these passive VG devices are less efficient in diminishing the shock displacement than an active control device—flow suction through a perforated plate placed in the interaction region—tested in a previous study for inlet buzz control [10]. Indeed, for a moderate value of the suction mass flow rate (equal to 20 g/s, which means around 1% of the channel mass flow rate), the decrease in shock oscillation amplitude is around 20% (from 30 to 24 mm). The very high RMS pressure level obtained with the G6 sensor is related to the presence of a recirculation bubble at this location, i.e., the rear part of the bump. Then, both spectra have the same behaviour with a 30 Hz fundamental peak and few harmonics almost at the same levels (see Fig. 12b). For the G3 sensor, discrepancies on the RMS pressure level are observed between the VG devices, this location corresponding to the

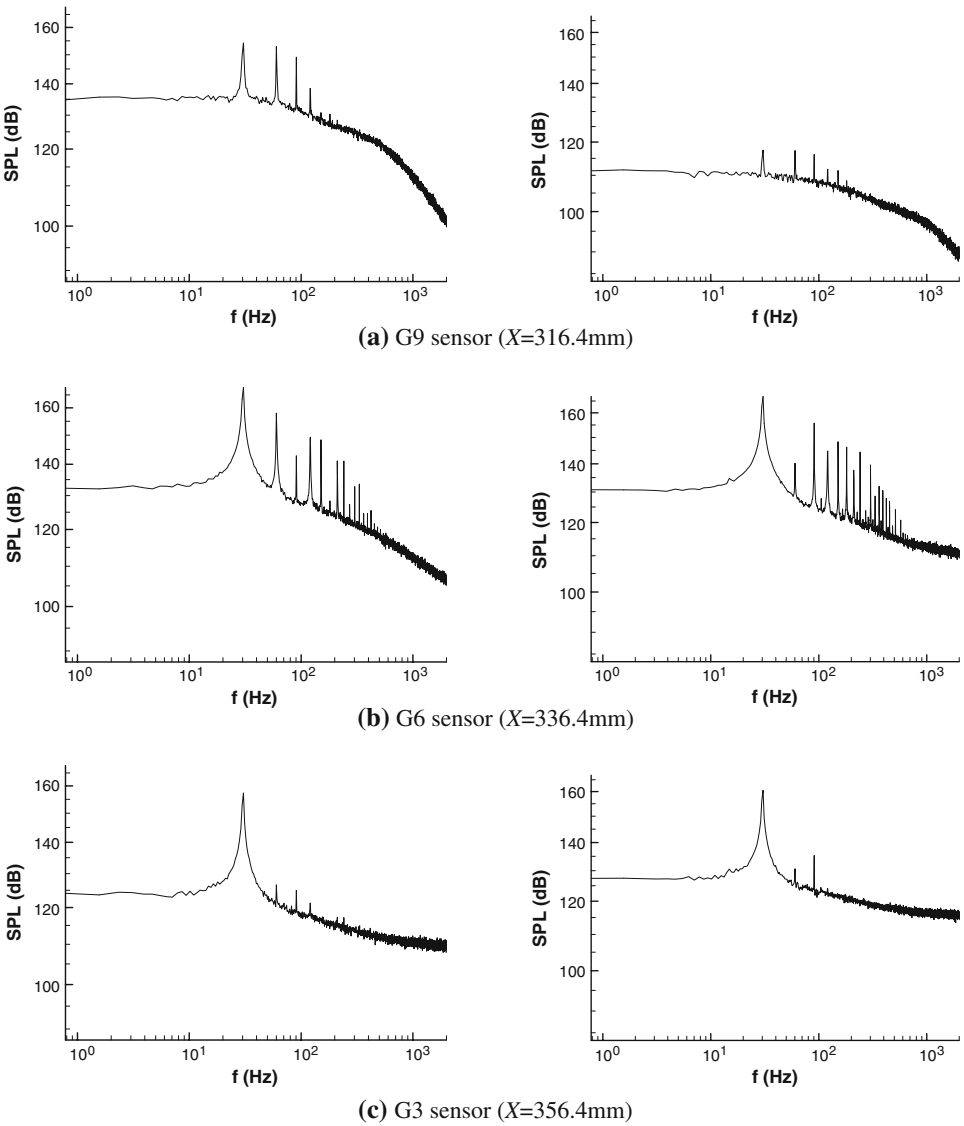

Fig. 12 Longitudinal evolution of the pressure fluctuations spectra for 30 Hz-forced shock oscillation configuration without control (*left*) and with VG-C2 device (*right*)

reattachment flow region. However, this sensor always being located downstream of the leading shock, the spectrum corresponding to the VG-C2 device has an equivalent behaviour to that of the reference case one (see Fig. 12c). The moderate RMS level remaining for the P2 sensor (compared to the upstream residual P1 level) means that the reattached boundary layer has not yet reached a new equilibrium state.

5 Conclusion

The aim of the experimental study was to control by mechanical vortex generator devices the strong interaction between a shock wave and a separated turbulent boundary layer in a transonic channel. Control devices—co-rotating and counter-rotating vane-type vortex generators—were implemented upstream of the shock foot region and tested both on a steady shock wave and on a forced shock oscillation configurations. Continuous and unsteady wall pressure measurements allowed to quantify the effects of vortex generators on the flow separation region and the shock oscillation amplitude. Laser sheet visualizations and oil flow visualizations permitted to track the trajectories of the small-scale streamwise vortices emanating from the vortex generator devices and their interaction with the boundary layer and the shock wave.

The spanwise spacing of vortex generator devices along the channel appeared to be an important parameter to control the flow separation region. When the distance between each device is decreased, the vortices merging is more efficient to reduce the separation. Moreover, their placement upstream of the shock wave is determinant to ensure that vortices have mixed momentum all spanwise long before they reach the separation line, so as to avoid separation cells. The expansion and compression waves generated by the vortex generators have a slight intensity. But in term of drag penalties, the way to reduce the effects of these perturbations should be to impose the height of the vortex generators at a value less than the sonic line of the incoming boundary layer.

Then, vortex generators reduced the amplitude of the forced shock wave oscillation by delaying the upstream displacement of the leading shock. Nevertheless, active control by flow suction through a perforated plate placed in the interaction region was more efficient to diminish the shock displacement.

Further investigations will be focused on the flowfield measurements in the main and spanwise directions by means of particule image velocimetry (PIV) technique, with emphasis near the wall to accurately determine the trajectories of vortices and the extension of the (residual) separation region. Laser sheet visualizations recorded on a high-speed camera will allow to point out the unsteady behaviour of vortices, especially after vortex merging in the interaction region. Control of corner flows will be tested to reduce the three-dimensionality of the flow and to see their impact on the separation benefit given by the vortex generators.

Acknowledgments The research reported here was undertaken as part of the UFAST project (Unsteady effects in shock wave induced separation) funded by the European Union.

References

1. Pearcey, H.H.: Shock induced separation and its prevention by design and boundary layer control. In: Lachmann, G.V. Boundary Layer and Flow Control, vol. 2, pp. 1312–1314. Pergamon, Oxford (1961)
2. Stanewsky, E.: Adaptive wing and flow control technology. Prog. Aero. Sci. **37**, 583–667 (2001)
3. Ashill, P.R., Fulker, J.L., Hackett, K.C.: A review of recent developments in flow control. Aeronaut. J. **109**, 205–232 (2005)
4. Lin, J.C.: Review of research on low-profile vortex generators to control boundary layer separation. Prog. Aero. Sci. **38**, 389–420 (2002)
5. McCormick, D.C.: Shock-boundary layer interaction control with low-profile vortex generators and passive cavity. AIAA Paper 92-0064, 30th AIAA Aerospace Sciences Meeting and Exhibit, Reno, NV (1992)
6. Ashill, P.R., Fulker, J.L., Hackett, K.C.: Research at DERA on sub boundary layer vortex generators (SBVGs). AIAA Paper 2001-0887, 39th AIAA Aerospace Sciences Meeting and Exhibit, Reno, NV (2001)
7. Babinsky, H., Makinson, N.J., Morgan, C.E.: Micro-vortex generator flow control for supersonic engine inlets. AIAA Paper 2007-0521, 45th AIAA Aerospace Sciences Meeting and Exhibit, Reno, NV (2007)
8. Galli, A.: Contrôle de l'oscillation d'une onde de choc en écoulement transsonique de canal. Ph. D. thesis, University of Provence Aix-Marseille I (2005)
9. Délery, J.: Analysis of the separation due to shock wave - turbulent boundary layer interaction in transonic flow. Aero. Res. **6**, 305–320 (1978)
10. Galli, A., Corbel, B., Bur, R.: Control of forced shock-wave oscillations and separated boundary layer interaction. Aero. Sci. Tech. **9**, 653–660 (2005)
11. Sajben, M., Bogar, T.J., Kroutil, J.: Forced oscillation experiments in supercritical diffuser flows. AIAA J. **22**, 465–474 (1984)
12. Salmon, J.T., Bogar, T.J., Sajben, M.: Laser Doppler velocimeter measurements in unsteady, separated, transonic diffuser flows. AIAA J. **21**, 1690–1697 (1983)
13. Ott, P., Bölcs, A., Fransson, T.: Experimental and numerical study of the time-dependent pressure response of a shock-wave oscillating in a nozzle. ASME J. Turbo. **117**, 106–114 (1995)
14. Pauley, W.R., Eaton, J.K.: Experimental study of the development of longitudinal vortex pairs embedded in a turbulent boundary layer. AIAA J. **26**, 816–823 (1988)
15. Godard, G., Stanislas, M.: Control of a decelerating boundary layer. Part 1: Optimization of passive vortex generators. Aero. Sci. Tech. **10**, 181–191 (2006)
16. Coudert, L.: Contrôle par générateurs de tourbillons d'une interaction onde de choc / couche limite avec décollement en écoulement transsonique. Master 2 report of University of Poitiers (2007)
17. Dandois, J., Brunet, V., Molton, P., Abart, J-C., Lepage, A.: Buffet Control by Means of Mechanical and Fluidic Vortex Generators. CEAS/KATnet II Conference, Bremen, Germany (2009)